Su *et al. Geoscience Letters* (2026) 13:16
https://doi.org/10.1186/s40562-026-00466-1

Geoscience Letters

RESEARCH Open Access

# Assessing drought changes in China under a $CO_2$ removal scenario

Xiaoyun Su[1], Lin Wang[2,4*], Gang Huang[2,3*] and Ting Wang[5]

**Abstract**
Understanding regional drought responses to $CO_2$ removal is critical for carbon-neutral pathways, yet remains poorly understood for China. To address this gap, we developed a bias-corrected and spatially downscaled SPEI dataset from multi-model $CO_2$ removal experiments to evaluate drought evolution, driving mechanisms, and event characteristics (frequency, duration, and severity) across China and its subregions. The results reveal a lagged drought response of 5–10 years to rapid $CO_2$ removal, after which conditions gradually improve. This mitigation is accompanied by less frequent, shorter-duration, and less severe drought events. Notably, extreme droughts show alleviation primarily through reduced persistence and intensity. Attribution analysis shows distinct regional controls: arid zones are dominated by potential evapotranspiration (PET), semi-arid and semi-humid regions by precipitation, while humid regions are jointly governed by precipitation and its nonlinear interaction with PET. Critically, even after $CO_2$ returns to pre-industrial levels, drought recovery is incomplete and regionally heterogeneous, with persistent residual effects in some areas contrasting with over-recovery in others. These findings highlight that climatic inertia fundamentally constrains $CO_2$ removal from rapidly reversing regional drought risks, while pronounced spatial heterogeneity necessitates region-specific adaptation strategies in designing carbon-neutral pathways.

**Keywords** $CO_2$ removal, Drought, SPEI, Bias correction and spatial downscaling, Attribution analysis

## Introduction

Drought is one of the most frequent and devastating natural disasters in China, exerting profound impacts on agricultural security, water resource management, and socioeconomic development (Chen et al. 2021; Wang et al. 2023; Xue et al. 2024). Severe droughts occur almost every year in China (Huang et al. 2023; Li et al. 2023). For instance, a prolonged winter-spring drought in Southwest China during 2009–2010 affected more than 20 million people and caused direct economic losses of approximately 30 billion USD (Yang et al. 2012). Similarly, Eastern China in summer 2013 (Xia et al. 2016) and North China in summer 2014 (Wang and He 2015) also experienced severe droughts. More recently, the record-breaking extreme heat and drought event in the Yangtze River Basin in 2022 affected nearly 40 million people and

*Correspondence:
Lin Wang
wang_lin@mail.iap.ac.cn; linwang@mail.iap.ac.cn
Gang Huang
hg@mail.iap.ac.cn
[1]Department of Mathematics, North University of China, Taiyuan 030051, China
[2]National Key Laboratory of Earth System Numerical Modeling and Application, Institute of Atmospheric Physics, Chinese Academy of Sciences, Beijing 100029, China
[3]College of Earth and Planetary Sciences, University of Chinese Academy of Sciences, Beijing 100049, China
[4]Temperate East Asia Research Center on Global Change, Institute of Atmospheric Physics, Chinese Academy of Sciences, Beijing 100029, China
[5]Laboratory of Middle Atmosphere and Global Environment Observation (LAGEO), Institute of Atmospheric Physics, Chinese Academy of Sciences, Beijing 100029, China

resulted in direct economic losses of 32.8 billion CNY (MEMC 2022). Projections suggest China's economic losses would reach ten times the historical baseline at 1.5 °C of warming, and several billion dollars more at 2 °C (Su et al. 2018). Therefore, a comprehensive assessment of future drought evolution under climate change scenarios is crucial for developing effective regional adaptation policies and ensuring national food and water security.

Under global warming, increased atmospheric water vapor content may intensify the hydrological cycle, leading to increases in both mean and extreme precipitation over China (Held and Soden 2006; Shu et al. 2024; Chen et al. 2024). However, enhanced evapotranspiration driven by rising temperatures may offset or even outweigh precipitation increases (Huang et al. 2023), resulting in more frequent and severe droughts across most regions in China (Wan et al. 2023; Xue et al. 2024). Since the beginning of the 21st century, drought events have intensified nationwide (Jin et al. 2025). While northern China remains drought-prone, southern China has also exhibited a pronounced drying tendency in recent decades (Han et al. 2021). If global warming continues, extreme droughts defined under present-day climate conditions are projected to become the future norm (Stevenson et al. 2022). Such drying trends are particularly evident over southern China and are primarily attributed to surface warming (Chen et al. 2023). The Yangtze River basin is expected to experience longer-lasting and more intense drought events (Su et al. 2021). Moreover, long-lasting and severe droughts are projected to become more frequent not only in Northwest and Central China (Xue et al. 2024), but also in the transitional climate zone (Piao et al. 2021).

To address climate change challenges, many countries have committed to achieving net-zero $CO_2$ emissions at various points this century (CAT 2025), with $CO_2$ removal (CDR) technologies viewed as a critical pathway toward achieving net-zero or even negative emission targets (Iyer et al. 2021; Kazemifar 2022; Smith et al. 2024). To advance scientific understanding of climate system responses under the CDR scenario, the Carbon Dioxide Removal Model Intercomparison Project (CDRMIP) was initiated (Keller et al. 2018). Previous studies have shown that climate responses to CDR are strongly modulated by the ocean's large thermal inertia (Wu et al. 2015; Kim et al. 2022; Cao et al. 2023), resulting in significant hysteresis and potential irreversibility during the negative $CO_2$ emissions phase—meaning the climate system may not fully recover within perceptible time scales. This feature is also evident in drought responses. Kim et al. ( 2023) demonstrated that, due to hemispheric asymmetries in the Hadley circulation, subtropical droughts associated with the circulation cannot be fully reversed by CDR. More than 11% of global land areas have experienced strongly irreversible drought changes, and an increase in potential evapotranspiration (PET) leads to the hysteretic drought response during the CDR period (Su et al. 2024; Mondal et al. 2025). In drought hotspots, agroecological drought is about 65% more severe during the CDR period than under an equivalent increase period, and only about 73% of the increased drought frequency is reversed (Liu et al. 2025). Moreover, enhanced soil moisture–temperature coupling under net negative emissions leads to more pronounced drying trends and drought characteristics (Mondal et al. 2024). While progress has been made in understanding global drought responses, studies focusing on regional drought responses remain limited, particularly for China (Su et al. 2025; Tang et al. 2025). Given China's commitment to achieving carbon neutrality by 2060, investigating drought changes under the CDR scenario holds both scientific and practical importance.

In this study, we utilize outputs from idealized CDR experiments within CDRMIP and apply bias correction and spatial downscaling (BCSD) techniques to construct a high-resolution SPEI dataset for China. Using this dataset, we systematically evaluate drought evolution across six subregions of China, including frequency, duration, and severity during the $CO_2$ ramp-up, ramp-down, and stabilization phases. Our analysis focuses on two key comparisons: (1) the differences between peak $CO_2$ conditions and post-removal stabilization to assess CDR effectiveness in potential drought mitigation, and (2) the differences between post-removal conditions and pre-industrial (PI) levels to evaluate the reversibility of drought changes. This comprehensive approach aims to deepen our knowledge of how regional drought patterns in China respond to CDR.

## Data and methods

### Study area

This study focuses on China as the primary research domain. Given its vast geographic extent and substantial regional climate variability, China is divided into six subregions (Fig. 1): Northwest China (NW: 35°–50° N, 73°–105° E), Southwest China (SW: 20°–35° N, 90°–105° E), Northeast China (NE: 42°–54° N, 105°–135° E), North China (NC: 35°–42° N, 105°–125° E), the Yangtze River Valley (YZ: 28°–35° N, 105°–123° E), and Southeast China (SE: 18°–28° N, 105°–120° E). This subdivision approach has been widely adopted in previous studies to better capture spatial heterogeneity and facilitate regional-scale analysis (Ma et al. 2015; Qiu et al. 2017; Li et al. 2021).

### Data

The observational data are drawn from the Climatic Research Unit (CRU) for monthly precipitation and PET at a 0.5° × 0.5° resolution (Harris et al. 2020). In addition, the model outputs are utilized from the Coupled

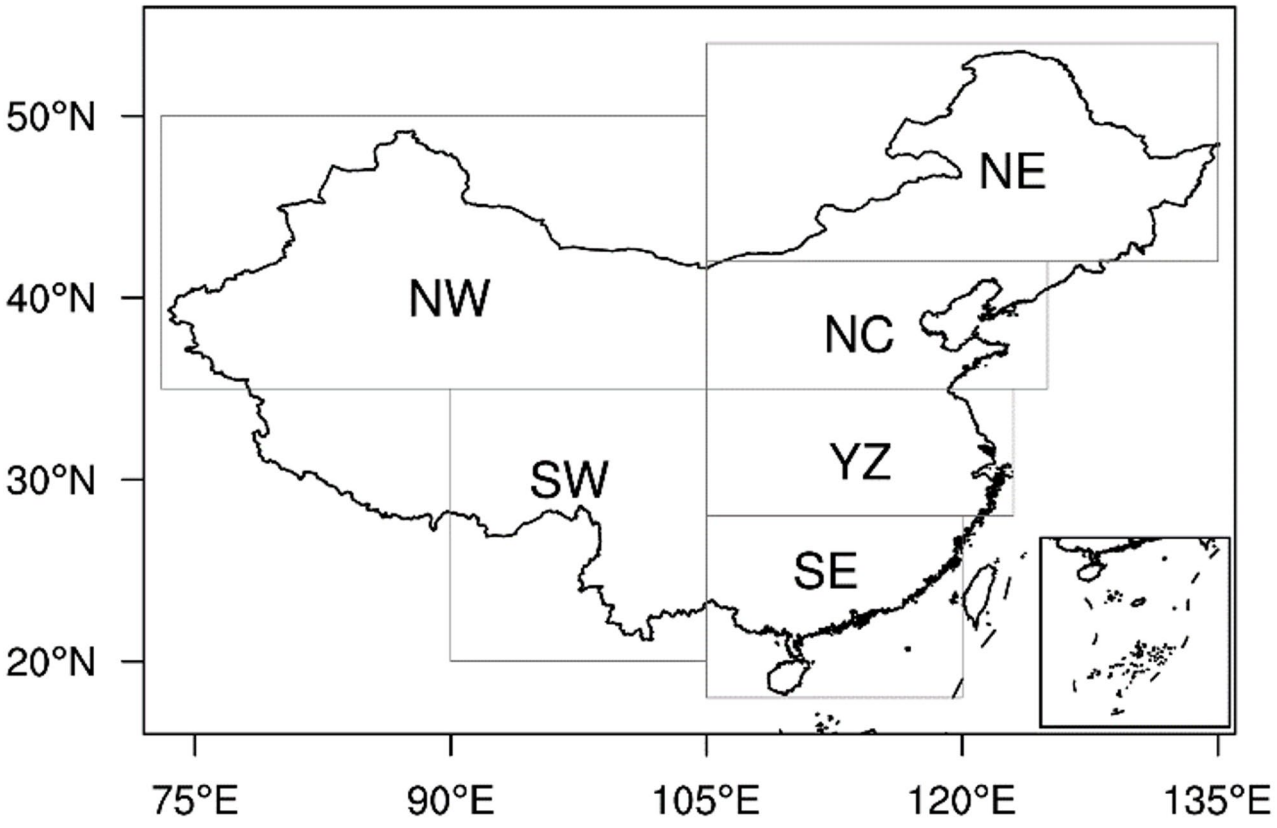


**Fig. 1** Six subregions of China

Model Intercomparison Project Phase 6 (CMIP6), including historical, piControl, 1pct$CO_2$, and 1pct$CO_2$-cdr experiments. In the 1pct$CO_2$ experiment, atmospheric $CO_2$ concentrations start from the PI level (284.7 ppm) and increase by 1% $yr^{-1}$ for 140 years until quadrupling (1138.8 ppm), followed by a symmetric decrease at the same rate for another 140 years, eventually returning to its initial levels (Fig. S1). It is subsequently held constant for at least 60 years. Throughout this period, $CO_2$ concentration is the only varying external forcing, while all other forcings remain fixed at their piControl levels. Five available global climate models (GCMs)—ACCESS-ESM1-5, CanESM5, CNRM-ESM2-1, GFDL-ESM4, and MIROC-ES2L—are selected for this study (Table S1) because other participating models lack the necessary output variables.

The year when $CO_2$ begins to increase is defined as Year 1. Thus, Years 1–140 correspond to the $CO_2$ ramp-up period, Years 141–280 to the $CO_2$ ramp-down period, and Years 281–340 to the $CO_2$ stabilization period. To investigate drought changes during the CDR period, we characterize them by quantifying differences between the stabilization (St, Years 281–340) climate state and the 20-year mean at peak $CO_2$ (Pk, Years 131–150). Furthermore, to assess the reversibility of regional drought conditions after $CO_2$ returns to its initial concentrations, we also compare the St period with the PI period (last 100 years of the piControl experiment), noting that both periods have identical $CO_2$ levels (Fig. S1).

### SPEI calculation

The Standardized Precipitation Evapotranspiration Index (SPEI), proposed by Vicente-Serrano et al. (2010), has been widely used in studies of drought evolution and spatiotemporal variability in China (Chen and Sun 2015; Su et al. 2021; Xu et al. 2024). SPEI can capture drought characteristics across multiple time scales and reflect the balance between precipitation and PET. Several methods exist for estimating PET (Thornthwaite 1948; Hargreaves and Samani 1985; Allen et al. 1994). The Penman-Monteith equation, recommended by the Food and Agriculture Organization (FAO), integrates multiple meteorological factors such as temperature, radiation, and wind speed, and has been widely applied in drought studies across China (Su et al. 2018, 2021; Zhou et al. 2020). The equation is expressed as:

$$PET = \frac{0.408\Delta\,(R_n - G) + \gamma\,\frac{900}{T+273}U_2(e_a - e_d)}{\Delta + \gamma\,(1 + 0.34U_2)}, \qquad (1)$$

where $\Delta$ is the slope of the saturated vapor pressure-temperature curve ($\mathrm{kPa\,^{\circ}C^{-1}}$); $R_n$ is the net

radiation $\left(\mathrm{MJ\,m^{-2}\,d^{-1}}\right)$; $G$ is the soil heat flux density $\left(\mathrm{MJ\,m^{-2}\,d^{-1}}\right)$; $\gamma$ is the psychrometric constant $(\mathrm{kPa\,^{\circ}C^{-1}})$; $T$ is the mean surface temperature (°C); $U_2$ is the wind speed at 2 m height $(\mathrm{m\,s^{-1}})$; and $e_a$ and $e_d$ are the saturated and actual vapor pressure $(\mathrm{kPa})$, respectively.

SPEI is derived by first computing the monthly water balance as the difference between precipitation and PET for month *i*:

$$D_i = P_i - PET_i, \tag{2}$$

then the calculated *Di* values are aggregated at different time scales as follows, where *n* is the calculated month and *k* is the chosen time scale,

$$D_n^k = \sum_{i=0}^{k-1} \left(P_{n-i} - PET_{n-i}\right), \quad n \geq k \tag{3}$$

The resulting *D* series is then fitted to Log-Logistic probability distribution:

$$F\left(x\right) = \left[1 + \left(\frac{\alpha}{x-\gamma}\right)^{\beta}\right]^{-1}, \tag{4}$$

where $\alpha$, $\beta$, and $\gamma$ are the scale, shape, and location parameters, estimated using the method of L-moments.

Finally, the SPEI can be obtained as the standardized values of *F(x)*:

$$\begin{cases} SPEI = W - \frac{C_0 + C_1 W + C_2 W^2}{1 + d_1 W + d_2 W^2 + d_3 W^3} & P \leq 0.5 \\ SPEI = -\left(W - \frac{C_0 + C_1 W + C_2 W^2}{1 + d_1 W + d_2 W^2 + d_3 W^3}\right) & P > 0.5 \end{cases}, \tag{5}$$

where $W = \sqrt{-2\ln P}$, $P = 1 - F\left(x\right)$ is the probability of exceeding a given *D* value, and the constants are $C_0 = 2.515517$, $C_1 = 0.802853$, $C_2 = 0.010328$, $d_1 = 1.432788$, $d_2 = 0.189269$, and $d_3 = 0.001308$.

### Bias correction and spatial downscaling

GCMs generally exhibit substantial systematic biases when applied at regional scales, which may lead to inaccurate assessments of regional climate change. To obtain reliable climate projections over China, it is therefore essential to apply appropriate bias correction techniques. In this study, we employ a quantile mapping approach, which adjusts the cumulative distribution function (CDF) of model outputs to match that of the reference observations. Specifically, we adopt the Equiratio Cumulative Distribution Function Matching (EQCDF) method proposed by Wang and Chen (2014a), which can be expressed as:

$$\widetilde{x}_{m-p,adjust} = x_{m-p} \cdot \frac{F_{o-c}^{-1}[F_{m-p}(x_{m-p})]}{F_{m-c}^{-1}[F_{m-p}(x_{m-p})]}, \tag{6}$$

where $x_{m-p}$ is the raw model projection, $\widetilde{x}_{m-p,adjust}$ is the bias-corrected value, $F_{m-p}$ is the CDF of the model projection, and $F_{o-c}^{-1}$ and $F_{m-c}^{-1}$ represent the quantile functions derived from observed and modeled historical data, respectively. Compared to the Equidistant Cumulative Distribution Function Matching (EDCDF) method proposed by Li et al. (2010), EQCDF effectively avoids the occurrence of negative values in precipitation and PET, and has been widely applied in climate impact studies (Wang and Chen 2014a, b; Piao et al. 2022). Estimation of the quantile functions $F_{o-c}^{-1} \cdot F_{m-p}$ and $F_{m-c}^{-1} \cdot F_{m-p}$ can be achieved using non-parametric methods, which do not require assumptions about the underlying data distribution and are therefore recommended (Gudmundsson et al. 2012).

To facilitate regional-scale analysis with different models, it is also necessary to unify the bias-corrected outputs to a common high spatial resolution. Statistical downscaling methods have several advantages, including flexibility, computational efficiency, and the ability to incorporate observed climatological patterns. The procedure is as follows: (1) high-resolution observational data are first aggregated to the coarse GCM resolution using an area-weighted averaging approach; (2) the ratio between the bias-corrected GCM output and the aggregated observational data is then computed to obtain a factor field; (3) this factor field is bilinearly interpolated onto the fine-resolution observational grid; and (4) the interpolated factor field is multiplied by the high-resolution observations to produce high-resolution GCM outputs. In this study, precipitation and PET data from the CRU are used as the observational reference, resulting in final GCM outputs with a spatial resolution of 0.5° × 0.5°. Further technical details regarding the BCSD procedures can be found in Wang and Chen (2014a).

Among the five GCMs used in this study, MIROC-ES2L has the coarsest spatial resolution. As an illustrative example, we present the precipitation fields from MIROC-ES2L for the period 1979–2014 after BCSD (Fig. 2). The results show that bias correction effectively reduces the model's systematic overestimation of precipitation over China, while spatial downscaling substantially enhances the effective resolution of the model outputs. This approach allows the global model to better capture regional climatic features in greater detail, providing more realistic representations of fine-scale processes.

### Attribution method

Since SPEI is jointly determined by precipitation and PET (Eqs. 2–3), a control-variable attribution approach is employed to quantify their contributions to SPEI

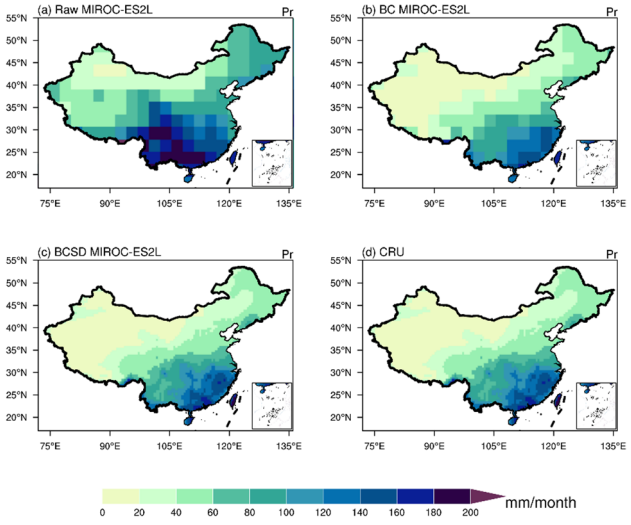


**Fig. 2** Climatological mean precipitation over China during 1979–2014 for **a** the raw MIROC-ES2L output, **b** the bias-corrected output, **c** the bias-corrected and spatially downscaled output, and **d** the CRU dataset (unit: mm month$^{-1}$)

variations during $CO_2$ concentration changes (Yin et al. 2023; Wang et al. 2024). This approach assumes that SPEI variations can be expressed as a linear superposition of contributions from precipitation, PET, and their joint effect. Accordingly, the contributions are quantified by solving the following equations:

$$SPEI\left(P_{CO_2}, PET_{PI}\right) - SPEI\left(P_{PI}, PET_{PI}\right) = C_P + C_{P\times PET}, \quad (7)$$

$$SPEI\left(P_{PI}, PET_{CO_2}\right) - SPEI\left(P_{PI}, PET_{PI}\right) = C_{PET} + C_{P\times PET}, \quad (8)$$

$$SPEI\left(P_{CO_2}, PET_{CO_2}\right) - SPEI\left(P_{PI}, PET_{PI}\right) = C_P + C_{PET} + C_{P\times PET}. \quad (9)$$

Here, the subscript *PI* denotes the baseline period defined as the last 100 years of the piControl experiment, and $CO_2$ denotes the $CO_2$-changing period. $C_P$, $C_{PET}$, and $C_{P\times PET}$ represent the contributions from precipitation changes, PET changes, and their joint effect, respectively. All precipitation and PET data are processed with BCSD.

### Drought identification and characteristics

The run theory is commonly applied to identify and characterize drought events (Yevjevich 1967). In this study, a drought event is defined as a period of at least three consecutive months with negative SPEI values, during which the lowest SPEI less than −1 (Guo et al. 2018; Su et al. 2021; Li et al. 2021). Extreme drought events are defined as periods of at least three consecutive months with SPEI < −2. Several metrics are then employed to describe drought characteristics. The mean drought duration (MDD) represents the average number of months between the onset and termination of drought events. The mean drought severity (MDS) is calculated as the average cumulative SPEI within each drought event (multiplied by −1 for convenience of interpretation). The mean drought frequency (MDF) denotes the average number of drought events per year over the specified period (Fig. S2).

## Results

### Spatial-temporal changes and attribution of SPEI

Figure 3 presents the annual evolutions of SPEI over China and its six subregions, revealing distinct regional

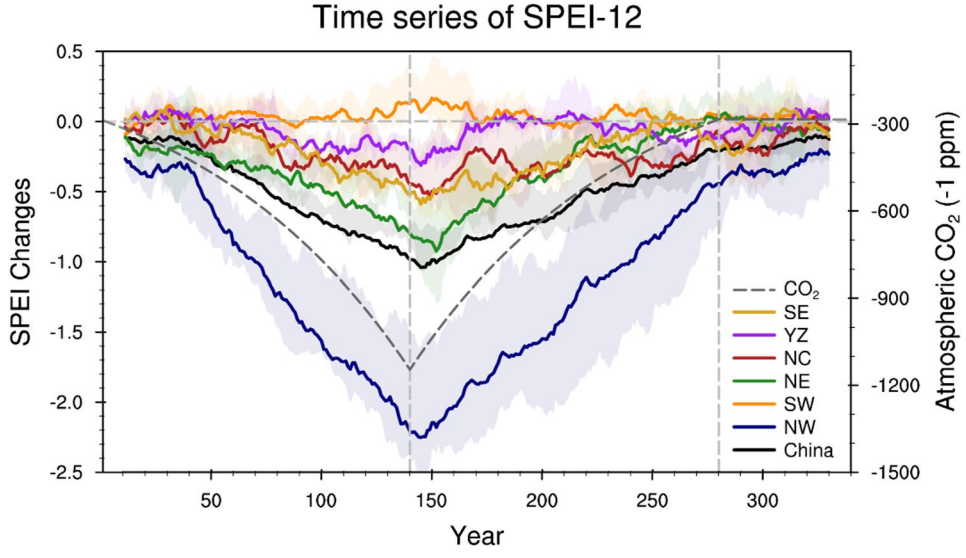


**Fig. 3** The 21-year running mean changes in the SPEI over China and its six subregions, together with atmospheric $CO_2$ concentration changes, relative to PI levels. Results are shown for the $CO_2$ ramp-up, ramp-down, and stabilization periods. The gray dashed line represents atmospheric $CO_2$ concentrations (multiplied by − 1 to facilitate comparison), while the colored solid lines and shading denote the multi-model mean (MME) and interquartile range across the five CMIP6 models, respectively

differences in response to atmospheric $CO_2$ changes. During the $CO_2$ ramp-up period, SPEI decreases across China, indicating overall drying. This trend is most pronounced in the NW and NE regions, moderate in the SE and NC regions, while the SW region exhibits a slight wetting trend. Following the rapid $CO_2$ decline, SPEI continues to decrease across China for several years before recovery, with most subregions exhibiting a similar lag of approximately 5–10 years. After $CO_2$ returns to PI levels, full drought recovery is not achieved. China-mean SPEI remains below its initial state, primarily due to persistent dryness in the NW region, with residual deficits also in the NC and SE regions. In contrast, spatial averages for the SW, YZ, and NE regions largely recover to their PI levels, although internal heterogeneity indicates incomplete local recovery (Fig. 4b).

Spatially, hydroclimatic conditions generally improve during the CDR period (Fig. 4a). The most pronounced recovery occurs in the arid NW region. It is noteworthy that in such water-limited environments, SPEI may overestimate drought severity, as actual evapotranspiration cannot increase proportionally with rising PET. Nevertheless, its directional trend remains a robust indicator of relative hydroclimatic change (Vicente-Serrano et al. 2011, 2015). To ensure that the large-magnitude changes in the NW region do not visually dominate the maps, non-uniform color scales are applied in Figs. 4 and 5. Beyond the NW region, the NE and SE regions also display a clear wetting trend, whereas parts of the NC and YZ regions shift toward drier conditions. In particular, the SW region experiences widespread drying, except for localized wetting in its southeast. After $CO_2$ returns to PI levels, full spatial recovery is not achieved (Fig. 4b). The NW, NC, and SE regions remain notably drier than baseline conditions. Although the spatial averages for the SW and NE regions largely recover, both exhibit pronounced internal heterogeneity (drier in the south, wetter in the north). In contrast, the YZ region essentially returns to its initial hydroclimatic state.

Based on a control-variable attribution method, we quantify the relative contributions of precipitation, PET, and their nonlinear interaction to SPEI changes (Figs. 5 and S3). During the $CO_2$ ramp-down period, precipitation contributes slightly more to China's overall wetting (42%) than PET (35%). However, the contribution structure varies substantially across subregions according to their background hydroclimatic conditions. In the arid NW region, SPEI changes are dominated by PET (62%), reflecting its high evaporative demand and limited water availability. By contrast, in the semi-arid to semi-humid transitional zones (the SW, NE, and NC regions) precipitation emerges as the primary driver (43–51%), where relatively higher moisture availability enhances SPEI sensitivity to precipitation changes compared to the NW region. In the humid YZ and SE regions, precipitation remains the leading contributor (46–48%). Notably, the nonlinear interaction between precipitation and PET accounts for a nearly equivalent share (37–43%), whereas the direct PET contribution is relatively small (11–15%). This indicates that drought variability in these humid areas is governed not only by precipitation supply but also by its synergistic coupling with evaporative demand. When $CO_2$ returns to PI levels, these regional attribution patterns remain largely stable, indicating consistent mechanistic controls throughout the $CO_2$ change. In summary, the dominant controls on SPEI changes align systematically with China's dry-wet gradient: PET prevails in arid regions, precipitation dominates in transitional zones, and both precipitation and its nonlinear interaction with PET are critical in humid regions.

### Changes in drought event characteristics

To assess how drought characteristics respond to CDR, we compare mean drought frequency, duration, and severity between the St and Pk periods across China and its six subregions (Fig. 6). While CDR leads to a nationwide reduction in drought frequency, duration, and severity, the degree of mitigation is region-dependent.

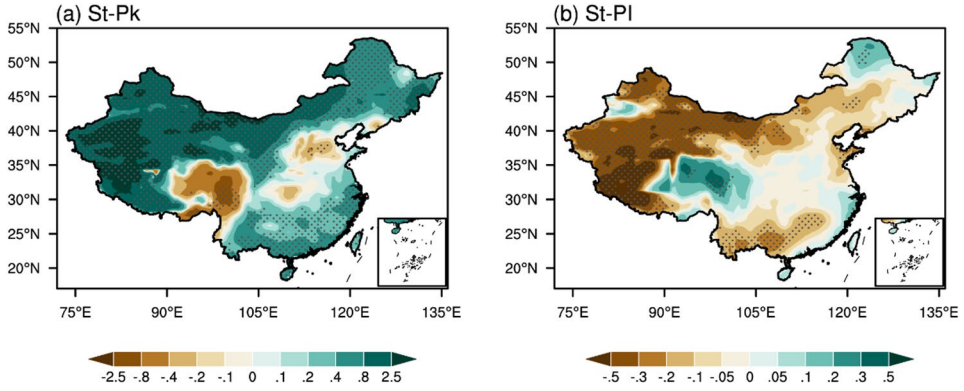


**Fig. 4** Spatial distribution of SPEI differences over China between **a** the St and Pk periods, and **b** the St and PI periods. Stippling indicates regions where at least four out of five models agree on the sign of the MME change, and the differences are statistically significant at the 90% confidence level

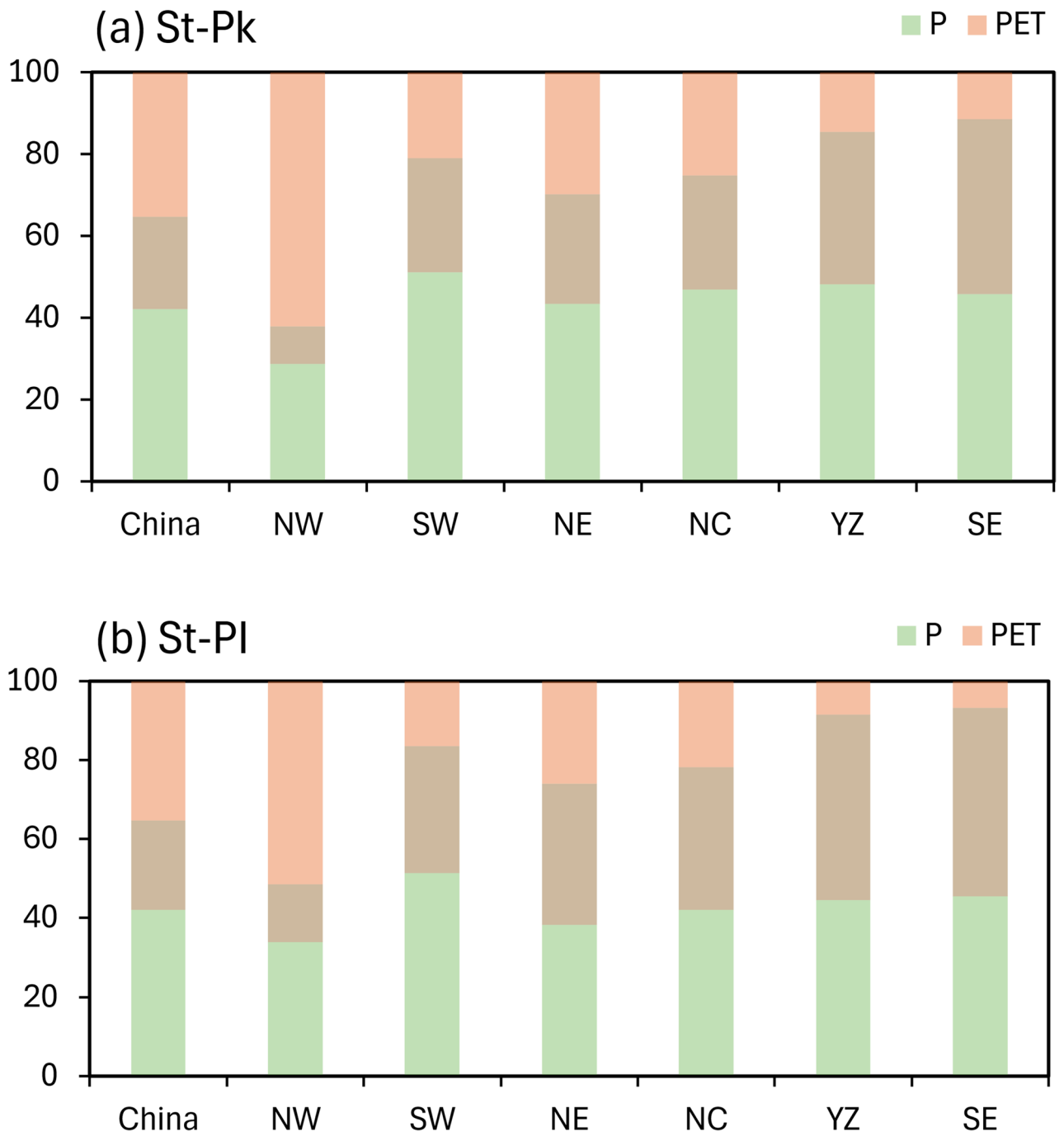


**Fig. 5** Contributions of precipitation (green), PET (orange), and their joint effects (brown) to SPEI differences between **a** the St and Pk periods, and **b** the St and PI periods over China and its subregions (unit: %)

Our analysis reveals that CDR implementation generally alleviates drought conditions, making events less frequent, shorter, and less severe. This mitigation, however, exhibits pronounced regional heterogeneity. Spatially, drought frequency decreases most substantially in western China, with the NW region showing the largest reduction (0.77 events $yr^{-1}$), consistent with its high sensitivity to hydroclimatic forcing. Reductions in eastern regions are more variable, being greatest in the NE (0.66 events $yr^{-1}$) and SE (0.46 events $yr^{-1}$) regions, but minimal in the NC and YZ regions. Correspondingly, drought duration shortens markedly in the NW (1.53 months $yr^{-1}$) and NE regions (0.74 months $yr^{-1}$), followed by moderate decreases in the SW and SE regions. Drought severity weakens across all regions, with the most significant declines again occurring in the NW (6.28 $yr^{-1}$) and

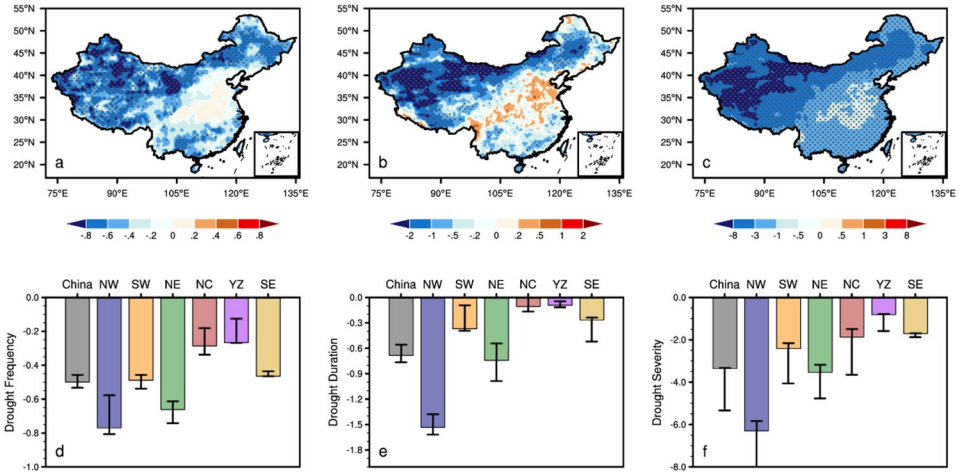


**Fig. 6** **a–c** Spatial differences in MDF, MDD, and MDS between St and Pk over China, and **d–f** their spatial averages over China and its subregions. Stippling in panels **a–c** indicates regions where at least four out of five models agree with the sign of the MME. Histograms and black vertical lines in panels **d–f** denote the multi-model median and interquartile range, respectively

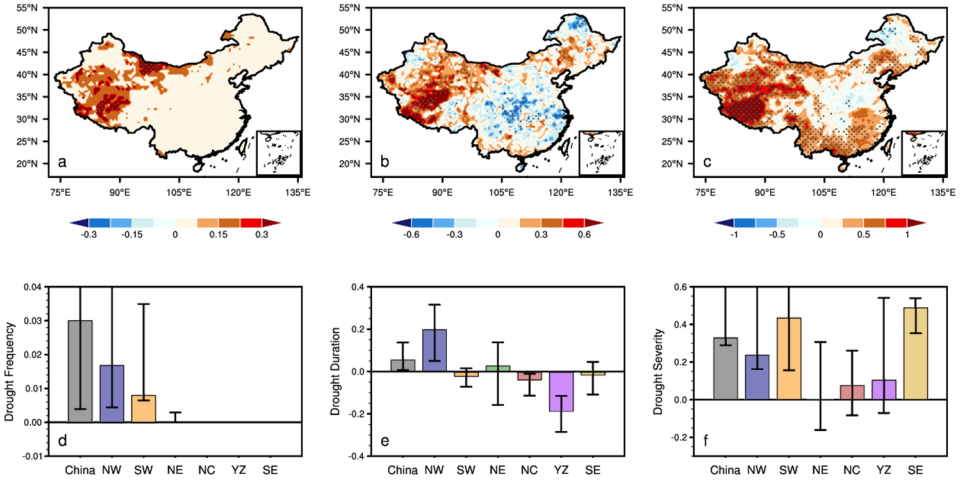


**Fig. 7** The same as Fig. 6, but for the differences between St and PI

NE (3.53 $yr^{-1}$) regions. Moderate reductions are observed in the SW, NC, and SE regions. In summary, CDR effectively mitigates drought across China, with the strongest benefits seen in the NW and NE regions, moderate effects in the SW and SE regions, and limited influence in the NC and YZ regions.

Given the severe risks posed by extreme droughts to ecosystems and society, we specifically analyze their behavior during the $CO_2$ ramp-down period (Fig. S4). The results reveal a distinct response pattern: while the frequency of extreme droughts shows a clear decrease only in the arid NW region—consistent with its high baseline susceptibility—other regions exhibit little change. In contrast, both the duration and severity of extreme droughts decrease significantly across most of China. This indicates that the alleviation of extreme drought under CDR is achieved primarily through shorter persistence and reduced intensity, rather than a drop in how often such events initiate. A notable exception is the NC region, where duration slightly increases even as severity weakens, highlighting that drought characteristics can shift in a compensatory manner. An exception occurs in the NC region, where duration slightly increases despite weakened severity, suggesting compensating changes among drought characteristics.

Furthermore, to evaluate whether drought characteristics fully recover after atmospheric $CO_2$ returns to PI levels, we compare the St and PI periods (Fig. 7). The analysis reveals widespread but spatially heterogeneous residual drying, indicating incomplete hydroclimatic reversibility. Drought frequency remains slightly elevated at the national scale (by 0.30 events $decade^{-1}$), with increases concentrated in western China—dominantly in the NW region but also locally in the SW region—while eastern China (the NE, NC, YZ, and SE regions) largely recovers to PI levels. For drought duration, the national

mean is prolonged (0.56 months decade$^{-1}$), again driven substantially by the NW region. A notable exception is the YZ region, where duration shortens considerably (1.88 months decade$^{-1}$), indicating over-recovery. The NE region exhibits a compensating north-south dipole, while the SW, NC, and SE regions show near-complete recovery. Drought severity strengthens across most regions, with the national mean exceeding PI levels by 3.29 decade$^{-1}$. Increases are pronounced in the SW (4.34 decade$^{-1}$), SE (4.90 decade$^{-1}$), and NW (2.38 decade$^{-1}$) regions. The NE region shows a north-south contrast in severity consistent with its duration pattern, whereas the NC and YZ remain moderately stronger. In summary, although many regions approach their PI conditions, residual drying signals persist—particularly in the NW, southern SW, and southern SE regions—manifesting as more frequent, prolonged, or severe droughts. This spatial heterogeneity underscores that even after CDR, regional drought risk may not return to baseline.

As $CO_2$ returns to PI levels, the recovery of extreme drought characteristics exhibits a clear dichotomy (Fig. S5). While the frequency of extreme droughts shows near-complete reversibility across China and its subregions, substantial residual anomalies persist in both duration and severity. Spatially, extreme drought duration remains prolonged, most notably in the NW, NE, and SE regions, in contrast to a shortening observed in the NC and YZ regions. Similarly, extreme drought severity remains elevated in the NW and SE regions, while approaching baseline levels elsewhere. These results indicate that even the occurrence rate of extreme droughts normalizes with $CO_2$ restoration, their persistence and intensity may retain a prolonged, regionally variable legacy.

## Conclusions

This study investigates drought evolution and recoverability over China under an idealized $CO_2$ removal scenario using a bias-corrected and spatially downscaled multi-model SPEI dataset. Changes in drought evolution, driving mechanisms, and event characteristics (frequency, duration, and severity) are examined for China and six subregions throughout the $CO_2$ change process.

Results show that $CO_2$ increase leads to widespread drying across China, while during rapid CDR, SPEI does not immediately reverse but continues to decline for several years before gradually recovering, indicating a pronounced lagged hydroclimatic response. As $CO_2$ is removed, drought frequency, duration, and severity generally weaken, with extreme droughts primarily alleviated through reductions in intensity and persistence rather than a substantial decrease in occurrence.

Attribution analysis reveals strong regional contrasts in the dominant drivers of SPEI changes. Drought variability in arid regions is primarily controlled by PET, semi-arid to semi-humid transition regions are mainly governed by precipitation, and humid regions are dominated by precipitation and its nonlinear interaction with PET. This contribution structure remains largely consistent in explaining the recoverability of drought after $CO_2$ returns to PI levels, suggesting a robust and stable attribution framework throughout $CO_2$ change.

When $CO_2$ returns to PI levels, drought conditions do not fully return to their baseline state across China. Residual enhancements in drought frequency, duration, or severity persist in several regions, although the YZ region exhibited an over-recovery in drought duration. This incomplete recovery highlights the role of climate system inertia and nonlinear processes, indicating that complete CDR to the PI level may be insufficient to rapidly restore regional drought risk.

Overall, CDR can substantially alleviate drought risk over China, but drought recovery varies substantially among regions. These findings underscore the need for region-specific adaptation strategies in future carbon-neutral pathways, with careful consideration of hydroclimatic inertia and irreversible risks.

## Discussion

The results of this study indicate that while $CO_2$ removal can effectively mitigate drought, the drought response exhibits obvious temporal lags and regional disparities. This reflects the inertia of the hydroclimatic system (Mondal et al. 2025) and the differential responses under varying background climatic conditions (Huang et al. 2023). Although $CO_2$ returns to PI levels, some drought conditions remain irrecoverable, particularly in terms of drought duration and severity.

To prevent the potential obscuring of drought frequency changes due to the merging and splitting of drought events based on event counts, we further employ the number of months under drought conditions to characterize drought frequency (Xu et al. 2021), in addition to event-based frequency. The results reveal important distinctions between these two metrics. During the $CO_2$ ramp-down period, both metrics show consistent decreases across China and its subregions (Fig. S6). However, after $CO_2$ returns to PI levels, notable regional discrepancies emerge: in some regions, event-based frequency recovers to baseline levels, yet the total months in drought remain elevated. Combined with changes in drought duration (Fig. 7), this suggests that in these regions, post-recovery drought variability is primarily controlled by event persistence rather than occurrence rate. This underscores the importance of employing multiple metrics to fully capture changes in drought characteristics under climate change scenarios.

However, this study also has some limitations. First, the highly idealized CDR scenario used here is primarily designed to amplify the response signal. More closely aligned with policy and realistic $CO_2$ pathways have been explored in recent studies (Zhong et al. 2025; Lu et al. 2025), which should be incorporated in future work. Second, this study directly applies bias correction to the model-calculated PET using CRU data as reference. Future efforts could consider correcting the individual input variables (e.g., temperature, radiation, wind speed) first, which would help to further disentangle the contributions of the underlying meteorological drivers (Sun et al. 2017; Su et al. 2024). Finally, regarding the mechanisms of drought change, our attribution analysis is limited to precipitation and PET. In reality, the processes influencing drought across China's diverse subregions are highly complex. For instance, the East Asian summer monsoon circulation is a critical factor for dryness/wetness in eastern China (Zhang and Wang 2022), while the Western Pacific subtropical high and the South Asian high are key circulation systems regulating summer precipitation (Xu et al. 2015; Ning et al. 2017). Sea surface temperature anomalies in different ocean basins—such as the El Niño–Southern Oscillation (Lv et al. 2022), the Pacific Decadal Oscillation (Zhu et al. 2015), the Indian Ocean Dipole (Zhou et al. 2021), and the Atlantic Multidecadal Oscillation (Si et al. 2021)—can influence dry/wet variations across different regions of China on various timescales. Future research should delve deeper into the specific processes driving drought changes in different subregions.

## Supplementary Information

The online version contains supplementary material available at https://doi.org/10.1186/s40562-026-00466-1.

Supplementary Material 1

**Acknowledgements**

The authors thank the two anonymous reviewers for their insightful and helpful comments on the original manuscript.

**Author contributions**

XS and LW conceived the study. SZ performed the data analysis, generated the figures, and drafted the manuscript. GH, LW, and TW supervised the research. GH and LW provided funding support. LW revised and refined the manuscript. All authors reviewed and approved the final version of the manuscript.

**Funding**

This work was supported by the National Key R&D Program of China, Project No. 2025YFF 0812000, the National Natural Science Foundation of China (Grants Nos. 42575036, 42530606, and 42261144687) and the International Partnership Program of Chinese Academy of Sciences for Future Network (Grant No. 060GJHZ2022104FN). We also thank for the technical support of the National Large Scientific and Technological Infrastructure "Earth System Numerical Simulation Facility" (https://cstr.cn/31134.02.EL).

**Data availability**

CRU TS4.07 precipitation and PET: https://data.ceda.ac.uk/badc/cru/data/cru_ts/cru_ts_4.07/data/pre. The CMIP6 outputs are available online at https://esgf-node.llnl.gov/search/cmip6/.

## Declarations

**Competing interests**

The authors declare no competing interests.

Received: 19 September 2025 / Accepted: 12 February 2026
Published online: 05 March 2026

**References**

Allen R, Smith M, Pereira L, Perrier A (1994) An update for the calculation of reference evaporation. ICID Bull 43:35–92

Cao L, Jin X-Y, Jiang J (2023) Simulated carbon cycle and earth system response to atmospheric $CO_2$ removal. Adv Clim Change Res 14:313–321. https://doi.org/10.1016/j.accre.2023.03.001

Chen H, Sun J (2015) Changes in drought characteristics over China using the standardized precipitation evapotranspiration index. J Clim 28:5430–5447. https://doi.org/10.1175/JCLI-D-14-00707.1

Chen L, Wang G, Miao L et al (2021) Future drought in CMIP6 projections and the socioeconomic impacts in China. Int J Climatol 41:4151–4170. https://doi.org/10.1002/joc.7064

Chen Q, Zhao T, Hua L et al (2023) Future drought changes in China projected by the CMIP6 models: contributions from key factors. J Meteorol Res 37:454–468. https://doi.org/10.1007/s13351-023-2169-8

Chen W, Cui H, Zwiers FW et al (2024) Detection and attribution of changes in precipitation extremes in China and its different climate zones. J Clim 37:5373–5385. https://doi.org/10.1175/JCLI-D-23-0770.1

Climate Action Tracker (CAT) (2022) CAT net zero target evaluations. https://climateactiontracker.org/global/cat-net-zero-target-evaluations/

Gudmundsson L, Bremnes JB, Haugen JE, Engen-Skaugen T (2012) Technical note: downscaling RCM precipitation to the station scale using statistical transformations—a comparison of methods. Hydrol Earth Syst Sci 16:3383–3390. https://doi.org/10.5194/hess-16-3383-2012

Guo H, Bao A, Liu T et al (2018) Spatial and Temporal characteristics of droughts in central Asia during 1966–2015. Sci Total Environ 624:1523–1538. https://doi.org/10.1016/j.scitotenv.2017.12.120

Han L, Zhang Q, Zhang Z et al (2021) Drought area, intensity and frequency changes in China under climate warming, 1961–2014. J Arid Environ 193:104596. https://doi.org/10.1016/j.jaridenv.2021.104596

Hargreaves GH, Samani ZA (1985) Reference crop evapotranspiration from temperature. Appl Eng Agric 1:96–99. https://doi.org/10.13031/2013.26773

Harris I, Osborn TJ, Jones P, Lister D (2020) Version 4 of the CRU TS monthly high-resolution gridded multivariate climate dataset. Sci Data 7:109. https://doi.org/10.1038/s41597-020-0453-3

Held IM, Soden BJ (2006) Robust responses of the hydrological cycle to global warming. J Clim 19:5686–5699. https://doi.org/10.1175/JCLI3990.1

Huang Y, Guo M, Bai P et al (2023) Warming intensifies severe drought over China from 1980 to 2019. Int J Climatol 43:1980–1992. https://doi.org/10.1002/joc.7957

Iyer G, Clarke L, Edmonds J et al (2021) The role of carbon dioxide removal in net-zero emissions pledges. Energy Clim Change 2:100043. https://doi.org/10.1016/j.egycc.2021.100043

Jin H, Zhang K, Zhang P et al (2025) Spatiotemporal evolution of drought status and its driving factors attribution in China. Sci Total Environ 958:178131. https://doi.org/10.1016/j.scitotenv.2024.178131

Kazemifar F (2022) A review of technologies for carbon capture, sequestration, and utilization: cost, capacity, and technology readiness. Greenh Gases 12:200–230. https://doi.org/10.1002/ghg.2131

Keller DP, Lenton A, Scott V et al (2018) The carbon dioxide removal model intercomparison project (CDRMIP): rationale and experimental protocol for CMIP6. Geosci Model Dev 11:1133–1160. https://doi.org/10.5194/gmd-11-1133-2018

Kim S-K, Shin J, An S-I et al (2022) Widespread irreversible changes in surface temperature and precipitation in response to $CO_2$ forcing. Nat Clim Chang 12:834–840. https://doi.org/10.1038/s41558-022-01452-z

Kim S-Y, Choi Y-J, Son S-W et al (2023) Hemispherically asymmetric Hadley cell response to CO2 removal. Sci Adv 9:eadg1801. https://doi.org/10.1126/sciadv.adg1801
Li H, Sheffield J, Wood EF (2010) Bias correction of monthly precipitation and temperature fields from intergovernmental panel on climate change AR4 models using equidistant quantile matching. J Geophys Research: Atmos 115. https://doi.org/10.1029/2009JD012882
Li W, Pan R, Jiang Z et al (2021) Future changes in the frequency of extreme droughts over China based on two large ensemble simulations. J Clim. https://doi.org/10.1175/JCLI-D-20-0656.1
Li M, Wang G, Zong S et al (2023) Copula-based assessment and regionalization of drought risk in China. Int J Environ Res Public Health 20:4074. https://doi.org/10.3390/ijerph20054074
Liu L, Hauser M, Windisch M, Seneviratne SI (2025) Hysteresis and reversibility of agroecological droughts in response to carbon dioxide removal. Nat Water https://doi.org/10.1038/s44221-025-00487-8
Lu Y, Jin L, Zhong J et al (2025) Earth system responses under a global 2 °C-target scenario aligned with China's carbon neutrality pledge. Environ Res Lett 20:104049. https://doi.org/10.1088/1748-9326/adfbfb
Lv A, Fan L, Zhang W (2022) Impact of ENSO events on droughts in China. Atmosphere 13:1764. https://doi.org/10.3390/atmos13111764
Ma S, Zhou T, Dai A, Han Z (2015) Observed changes in the distributions of daily precipitation frequency and amount over China from 1960 to 2013. J Clim. https://doi.org/10.1175/JCLI-D-15-0011.1
Ministry of Emergency Management of People's Republic of China (MEMC) (2022) Monthly National Natural Disasters in August 2022. https://www.mem.gov.cn/xw/yjglbgzdt/202209/t20220917_422674.shtml
Mondal SK, An S-I, Min S-K et al (2024) Enhanced soil moisture–temperature coupling could exacerbate drought under net-negative emissions. Npj Clim Atmos Sci 7:1–12. https://doi.org/10.1038/s41612-024-00820-0
Mondal SK, An S-I, Min S-K et al (2025) Hysteresis and irreversibility of global drought patterns in response to $CO_2$ mitigation efforts. Environ Res Lett 20:084047. https://doi.org/10.1088/1748-9326/ade608
Ning L, Liu J, Wang B (2017) How does the South Asian high influence extreme precipitation over Eastern China? J Geophys Res Atmos 122:4281–4298. https://doi.org/10.1002/2016JD026075
Piao J, Chen W, Chen S et al (2021) Mean States and future projections of precipitation over the monsoon transitional zone in China in CMIP5 and CMIP6 models. Clim Change 169:35. https://doi.org/10.1007/s10584-021-03286-8
Piao J, Chen W, Wang L, Chen S (2022) Future projections of precipitation, surface temperatures and drought events over the monsoon transitional zone in China from bias-corrected CMIP6 models. Int J Climatol 42:1203–1219. https://doi.org/10.1002/joc.7297
Qiu S, Zhou W, Leung MY-T, Li X (2017) Regional moisture budget associated with drought/flood events over China. Prog Earth Planet Sci 4:36. https://doi.org/10.1186/s40645-017-0148-3
Shu Z, Jin J, Zhang J et al (2024) 1.5℃ and 2.0℃ of global warming intensifies the hydrological extremes in China. J Hydrol 635:131229. https://doi.org/10.1016/j.jhydrol.2024.131229
Si D, Jiang D, Hu A, Lang X (2021) Variations in northeast Asian summer precipitation driven by the Atlantic multidecadal oscillation. Int J Climatol 41:1682–1695. https://doi.org/10.1002/joc.6912
Smith SM, Geden O, Gidden MJ et al (2024) The state of carbon dioxide removal-2nd Edition. https://doi.org/10.17605/OSF.IO/F85QJ
Stevenson S, Coats S, Touma D et al (2022) Twenty-first century hydroclimate: a continually changing baseline, with more frequent extremes. Proc Natl Acad Sci USA 119:e2108124119. https://doi.org/10.1073/pnas.2108124119
Su B, Huang J, Fischer T et al (2018) Drought losses in China might double between the 1.5 and 2.0 °C warming. Proc Natl Acad Sci 115:10600–10605. https://doi.org/10.1073/pnas.1802129115
Su B, Huang J, Mondal SK et al (2021) Insight from CMIP6 SSP-RCP scenarios for future drought characteristics in China. Atmos Res 250:105375. https://doi.org/10.1016/j.atmosres.2020.105375
Su X, Huang G, Wang L, Wang T (2024) Global drought changes and attribution under carbon neutrality scenario. Clim Dyn. https://doi.org/10.1007/s00382-024-07310-2
Su X, Wang L, Huang G et al (2025) Summer precipitation responses to $CO_2$ removal scenario over the transitional climate zone in East Asia and the driving mechanisms. Clim Dyn 63:153. https://doi.org/10.1007/s00382-025-07647-2
Sun S, Chen H, Sun G et al (2017) Attributing the changes in reference evapotranspiration in Southwestern China using a new separation method. J Hydrometeorol 18:777–798. https://doi.org/10.1175/JHM-D-16-0118.1
Tang B, Hu W, Duan A et al (2025) Asymmetric response of precipitation extremes in China to CO2 removal forcing. Environ Res Lett 20:074015. https://doi.org/10.1088/1748-9326/addedf
Thornthwaite CW (1948) An approach toward a rational classification of climate. Geogr Rev 38:55–94. https://doi.org/10.2307/210739
Vicente-Serrano SM, Beguería S, López-Moreno JI (2010) A multiscalar drought index sensitive to global warming: the standardized precipitation evapotranspiration index. J Clim 23:1696–1718. https://doi.org/10.1175/2009JCLI2909.1
Vicente-Serrano SM, Beguería S, López-Moreno JI (2011) Comment on characteristics and trends in various forms of the Palmer drought severity index (PDSI) during 1900–2008 by Aiguo Dai. J Geophys Res 116:D19112. https://doi.org/10.1029/2011JD016410
Vicente-Serrano SM, Van der Schrier G, Beguería S et al (2015) Contribution of precipitation and reference evapotranspiration to drought indices under different climates. J Hydrol 526:42–54. https://doi.org/10.1016/j.jhydrol.2014.11.025
Wan L, Ben VA, Qu Y, et al (2023) Drought characteristics and dominant factor-sacross China: Insights from high resolution daily SPEI dataset between 1979 and2018. Science of The Total Environment Sci Total Environ 901:166362 https://doi.org/10.1016/j.scitotenv.2023.166362
Wang L, Chen W (2014a) A CMIP5 multimodel projection of future temperature, precipitation, and climatological drought in China. Int J Climatol 34:2059–2078. https://doi.org/10.1002/joc.3822
Wang L, Chen W (2014b) Equiratio cumulative distribution function matching as an improvement to the equidistant approach in bias correction of precipitation. Atmospheric Sci Lett 15:1–6. https://doi.org/10.1002/asl2.454
Wang H, He S (2015) The North China/Northeastern Asia severe summer drought in 2014. J Clim 28:6667–6681. https://doi.org/10.1175/JCLI-D-15-0202.1
Wang X, Luo P, Zheng Y et al (2023) Drought disasters in China from 1991 to 2018: analysis of spatiotemporal trends and characteristics. Remote Sens 15:1708. https://doi.org/10.3390/rs15061708
Wang L, Chen W, Haung G et al (2024) Characteristics of super drought in Southwest China and the associated compounding effect of multiscalar anomalies. Sci China Earth Sci. https://doi.org/10.1007/s11430-023-1341-4
Wu P, Ridley J, Pardaens A et al (2015) The reversibility of $CO_2$ induced climate change. Clim Dyn 45:745–754. https://doi.org/10.1007/s00382-014-2302-6
Xia J, Tu K, Yan Z, Qi Y (2016) The super-heat wave in Eastern China during July–August 2013: a perspective of climate change. Int J Climatol 36:1291–1298. https://doi.org/10.1002/joc.4424
Xu Z, Fan K, Wang H (2015) Decadal variation of summer precipitation over China and associated atmospheric circulation after the late 1990s. J Clim 28:4086–4106. https://doi.org/10.1175/JCLI-D-14-00464.1
Xu D, Zhang Q, Ding Y, Zhang D (2021) Spatiotemporal pattern mining of drought in the last 40 years in China based on the SPEI and Space–Time cube. https://doi.org/10.1175/JAMC-D-21-0049.1
Xu F, Qu Y, Bento VA et al (2024) Understanding climate change impacts on drought in China over the 21st century: a multi-model assessment from CMIP6. Npj Clim Atmos Sci 7:32. https://doi.org/10.1038/s41612-024-00578-5
Xue R, Sun B, Li W et al (2024) Future projections of meteorological, agricultural and hydrological droughts in China using the emergent constraint. J Hydrology: Reg Stud 53:101767. https://doi.org/10.1016/j.ejrh.2024.101767
Yang J, Gong D, Wang W et al (2012) Extreme drought event of 2009/2010 over Southwestern China. Meteorol Atmos Phys 115:173–184. https://doi.org/10.1007/s00703-011-0172-6
Yevjevich V (1967) An objective approach to definitions and investigations of continental hydrologic droughts. Hydrology Paper No.23. Colorado State University, Colorado.
Yin Z, Yang S, Wei W (2023) Quantitative attribution of vertical motions responsible for the early spring drought conditions over southeastern China. Clim Dyn 61:2655–2672. https://doi.org/10.1007/s00382-023-06708-8
Zhang Q, Wang Y (2022) Distribution of hazard and risk caused by agricultural drought and flood and their correlations in summer monsoon–affected areas of China. Theor Appl Climatol 149:965–981. https://doi.org/10.1007/s00704-022-04093-6
Zhong J, Zhang X, Zhang D et al (2025) Plausible global emissions scenario for 2 °C aligned with china's net-zero pathway. Nat Commun 16:8102. https://doi.org/10.1038/s41467-025-62983-5

Zhou J, Wang Y, Su B et al (2020) Choice of potential evapotranspiration formulas influences drought assessment: a case study in China. Atmos Res 242:104979. https://doi.org/10.1016/j.atmosres.2020.104979

Zhou Z-Q, Xie S-P, Zhang R (2021) Historic Yangtze flooding of 2020 tied to extreme Indian ocean conditions. PNAS 118:e2022255118. https://doi.org/10.1073/pnas.2022255118

Zhu Y, Wang H, Ma J et al (2015) Contribution of the phase transition of pacific decadal oscillation to the late 1990s' shift in East China summer rainfall. J Geophys Res Atmos 120:8817–8827. https://doi.org/10.1002/2015JD023545

## Publisher's note